

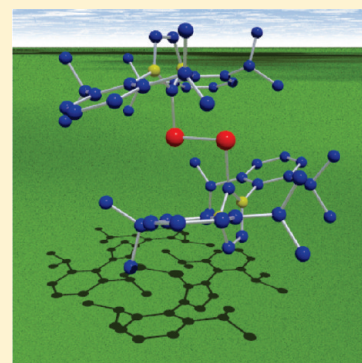
Carbene Stabilization of Highly Reactive Main-Group Molecules

Yuzhong Wang and Gregory H. Robinson*

Department of Chemistry, The University of Georgia, Athens, Georgia 30602-2556, United States

Supporting Information

ABSTRACT: This article highlights recent efforts of this laboratory in the stabilization of highly reactive, low-oxidation-state, main-group molecules using bulky N-heterocyclic carbene ligands [L: = :C{N(2,6-Prⁱ₂C₆H₃)CH}₂; L': = :C{N(2,4,6-Me₃C₆H₂)CH}₂; L'': = :C{(i-Pr)NC(Me)}₂]. The syntheses, structures, and computational studies of carbene-stabilized neutral diborenes [L:(H)B=B(H):L and L':(H)B=B(H):L'], a neutral Ga₆ octahedron (L':Ga[Ga₄Mes₄]Ga:L''), disilicon (L:Si=Si:L), bis-silylene [L:(Cl)Si-Si(Cl):L], dipnictogens (L:E-E:L, E = P, As; L':P-P:L'), and parent phosphinidene (L:PH) are discussed. Some of the unique challenges associated with this “carbene-stabilization” strategy are also presented.



INTRODUCTION

The significant advances in low-oxidation-state main-group chemistry over the past few decades have yielded a number of iconic molecules.^{1–3} The choice of ligand, as is often the case, has proven critical in the synthesis of these compounds. Sterically demanding, (formally) anionic ligands have been extensively utilized in the synthesis of these molecules. Arguably, *m*-terphenyl ligands have been the most prolific ligands in this regard.^{4–7} Some years ago, chemists began to utilize neutral donor ligands in this strategy.^{8,9} Notably, the “neutral” character of these types of donor ligands grants access to compounds containing main-group elements in the formal oxidation state of zero. To this end, N-heterocyclic carbenes (NHCs), discovered by Arduengo et al.¹⁰ and extensively utilized in organic and transition-metal catalysis,¹¹ are attractive in this regard. Indeed, we have witnessed remarkable progress in carbene-based main-group chemistry.^{12–14} In this article, we highlight the syntheses, structures, and computational studies of NHC-stabilized, low-oxidation-state, main-group molecules that were recently discovered in our laboratory. These carbene-stabilized main-group molecules with unusually low oxidation states not only exhibit structural novelty but also provide a unique platform from which novel main-group molecules may be further accessed.

SELECTION OF NHC LIGANDS

Over the past two decades, NHCs has considerably extended.¹⁵ Among these, ligands **I** (L: = :C{N(2,6-Prⁱ₂C₆H₃)CH}₂), **II** (L': = :C{N(2,4,6-Me₃C₆H₂)CH}₂), and **III** (L'': = :C{(i-Pr)NC(Me)}₂) are particularly attractive (Scheme 1).^{16,17}

The 2,6-diisopropylphenyl substituents in **I** and the mesityl substituents in **II** provide significant steric bulk about the carbene

center, while the isopropyl groups of **III** afford considerably less bulk. It is also significant that ligands **I**, **II**, and **III** contain aromatic five-membered imidazole rings and are expected to be more robust under harsh reaction conditions than ligands **IV**, **V**, and **VI**, which contain a saturated, nonaromatic C₃N₂ ring. The reactions of lithium metal with **I** and **IV** clearly illustrate this point: the former results in a lithiated carbene ligand [**VII**, an anionic N-heterocyclic dicarbene because it exhibits dicarbene character at both the C(2) and C(4) centers],^{18,19} while the latter affords a ring-cleaved product **VIII** (Scheme 2).²⁰

The X-ray structure of **VIII** (Figure 1) confirms that lithium reduction of **IV** led to a lithiated amidine ligand (**VIII**) through cleavage of the C–N bonds and the coupling reaction between the carbene carbon [C(1)] and the benzylic carbon [C(8)] in **IV**.

NHC-EX_n COMPLEXES

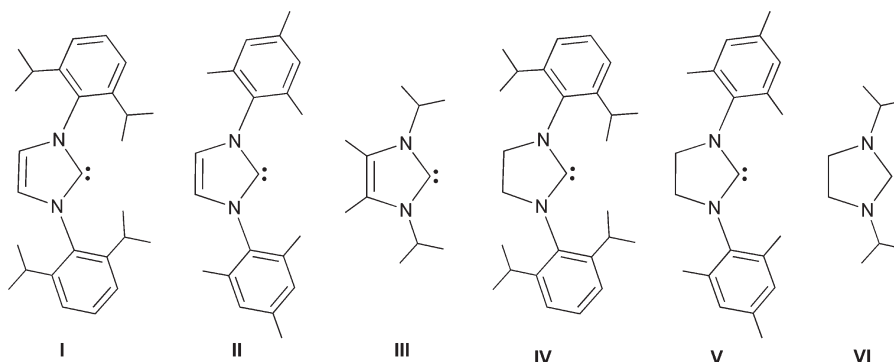
The room temperature reaction of NHCs with EX_n (E = B, Si, P, or As; X = Br or Cl; n = 3 or 4) in hexane results in the quantitative preparation of carbene-EX_n complexes (Scheme 3).^{21–26} In contrast to the boron complexes (**1** and **2**), the silicon, phosphorus, and arsenic complexes (**3–7**) are hypervalent compounds. The molecular structures of compounds **1**, **3**, **4**, and **6** are given in Figure 2.

The boron atom in compound **1** is four-coordinate and adopts a tetrahedral geometry.²¹ The B–C single bond distance in **1** [1.623(7) Å] is 0.03 Å longer than that of L:BX₃ [L: = **I**; 1.585(4) Å]. In hypervalent **3**,²³ the carbene resides in an equatorial site, with the four chlorine atoms completing the

Received: April 1, 2011

Published: June 02, 2011

Scheme 1. Typical NHCs



Scheme 2. Reaction of Lithium with I and IV

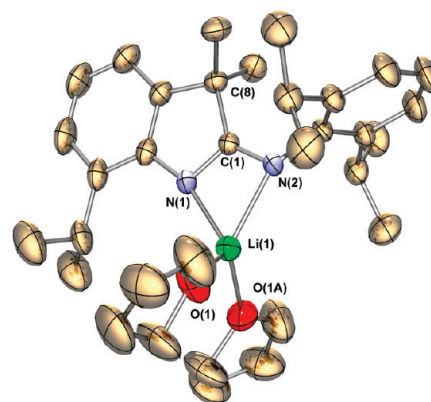
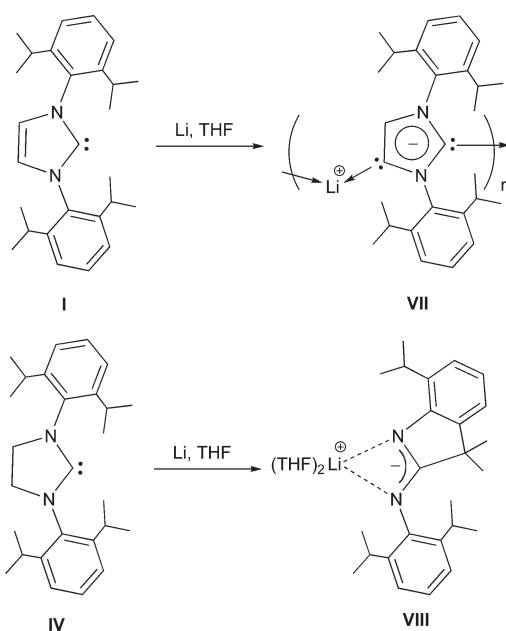
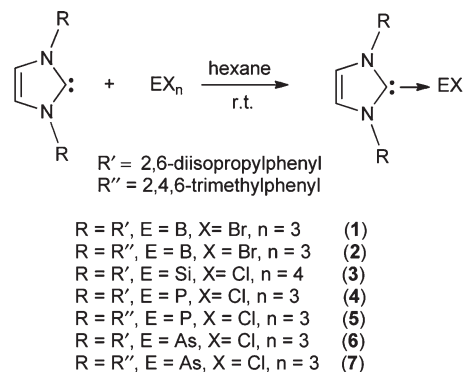


Figure 1. Molecular structure of VIII (thermal ellipsoids represent 30% probability; hydrogen atoms are omitted for clarity). Selected bond distances (Å) and angles (deg): Li(1)–N(1) 1.995(5), Li(1)–N(2) 2.141(5), Li(1)–O(1) 1.958(3), N(1)–C(1) 1.353(3), N(2)–C(1) 1.319(3), C(1)–C(8) 1.560(3); O(1)–Li(1)–O(1A) 108.9(3), N(1)–Li(1)–N(2) 66.87(16), N(1)–C(1)–N(2) 117.3(2), N(1)–C(1)–C(8) 111.4(2), N(2)–C(1)–C(8) 131.3(2).

trigonal-bipyramidal coordination of silicon. The Si–C bond distance in **3** [1.928(2) Å] compares well to that in L:SiCl₄ [1.911(7) Å; L: = :C{EtNC(Me)}₂]²⁷ and L:SiCl₂ [1.985(4) Å; L: = I].²⁸ The axial Si–Cl bond distances [$d_{\text{Si}(1)-\text{Cl}(2)} = d_{\text{Si}(1)-\text{Cl}(2A)} = 2.1892(5)$ Å] are about 0.12 Å longer than those [2.0696(6) Å] of the equatorial ones. Perhaps expectedly, compounds **4** and **6** are isostructural.^{24–26} While the central atom (phosphorus for **4**; arsenic for **6**) is four-coordinate, the coordination about the central atom adopts a seesaw orientation. In both cases, while two chlorine atoms reside at axial positions, one C_{NHC} atom, one chlorine atom, and one lone pair of electrons occupy the three equatorial sites. Notably, unlike **3**, the two axial E–Cl (E = P or As) bond distances differ considerably [$d_{\text{P}(1)-\text{Cl}(2)} = 2.471$ Å (av), $d_{\text{P}(1)-\text{Cl}(3)} = 2.238$ Å (av); $d_{\text{As}(1)-\text{Cl}(2)} = 2.484(2)$ Å, $d_{\text{As}(1)-\text{Cl}(3)} = 2.359(2)$ Å], which are longer than that in the equatorial plane [$d_{\text{P}(1)-\text{Cl}(1)} = 2.032$ Å (av); $d_{\text{As}(1)-\text{Cl}(1)} = 2.171(1)$ Å]. Both the P–C bond distance of 1.871(11) Å in **4** and the As–C bond distance of 2.018(3) Å in **6** are consistent with the corresponding single bonds.

Scheme 3. Synthesis of NHC-EX_n Complexes

NHC-STABILIZED NEUTRAL DIBORENES

In contrast to the ubiquitous homonuclear multiple-bond chemistry of its group 14 neighbor carbon, boron is best known for its electron-deficient borane clusters.²⁹ Both the first structurally characterized radical anion containing a one-electron π -bond, [Mes₂BB(Mes)Ph]^{•−},³⁰ and the first diborane dianion containing

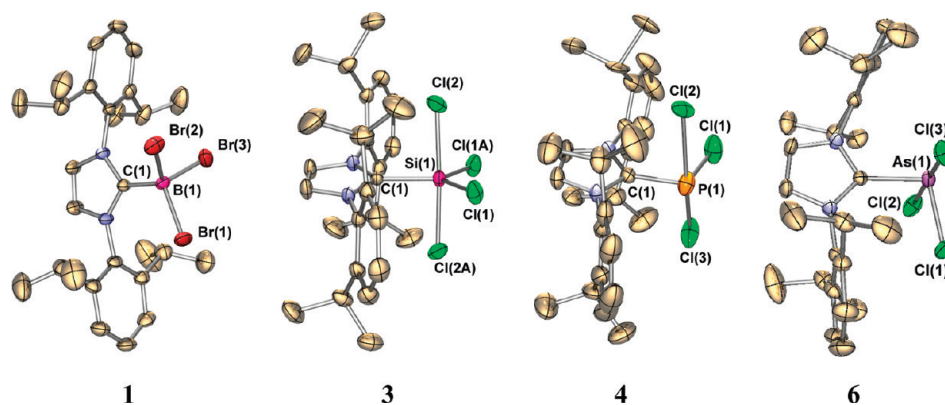
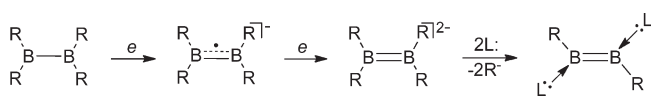


Figure 2. Molecular structures of L:BR₃ (1), L:SiCl₄ (3), L:PCl₃ (4), and L:AsCl₃ (6) (L: = I; hydrogen atoms are omitted for clarity).

Scheme 4. Evolution of B–B Multiple Bonds



a B–B double bond, [Mes₂B=B(Mes)Ph]²⁻,³¹ were reported by Power and co-workers more than a decade ago. Each three-coordinate boron atom in these two interesting compounds bonds to two (formally) anionic ligands (in addition to the other boron atom). In order to achieve the π -bond in these systems, one or two additional electrons had to be “added” to the respective neutral diborene(4) precursors by alkali-metal reduction, thus rendering their anionic character. Thus, to construct a neutral molecule containing a B=B double bond, one R⁻ group of each boron in [R₂B=BR₂]²⁻ would have to be replaced by a neutral Lewis base ligand L: (L: = CO, PR₃, or NHC; Scheme 4).^{21,32,33}

The potassium graphite reduction of **1** in diethyl ether afforded both an air-sensitive, crystalline red, neutral diborene, L:(H)B=B(H):L (**8**), and an air-stable colorless, crystalline diborene, L:(H)₂B–B(H)₂:L (**9**; Scheme 5).²¹ When the less sterically demanding carbene ligand **II** was employed in this synthetic strategy, the corresponding compounds L':(H)B=B(H):L' (**10**) and L':(H)₂B–B(H)₂:L' (**11**) (L': = **II**) were isolated.²² Notably, the aluminum analogues of diboranes **9** and **11** have recently been synthesized by reducing L:AlH₃ with a RMg–MgR (R = [(MesNCMe)₂CH]⁻) compound, which exhibits a structure similar to those of diboranes **9** and **11**.³⁴

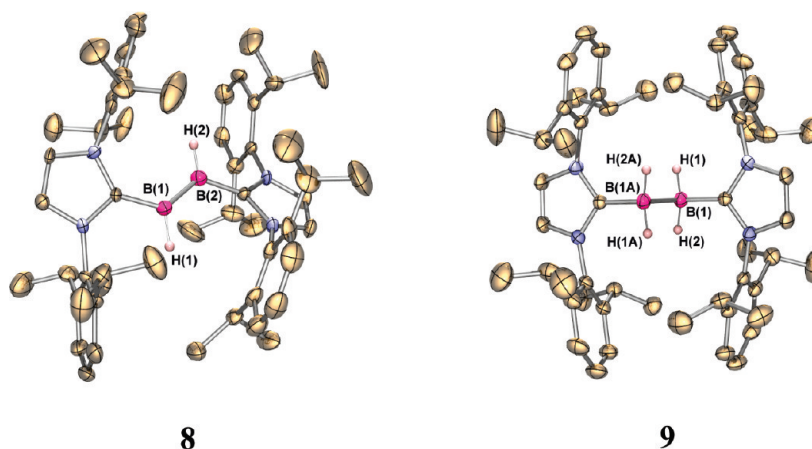
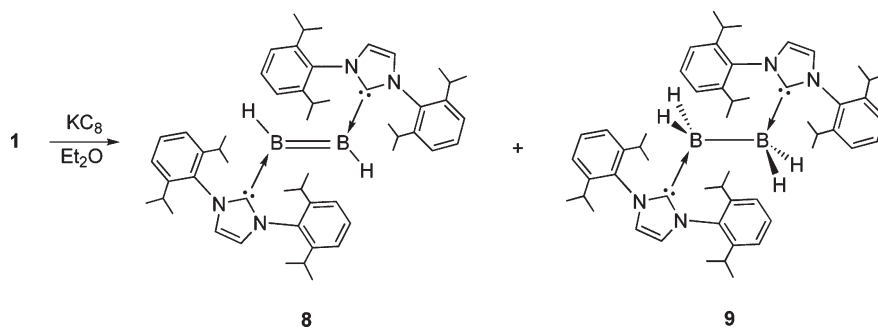
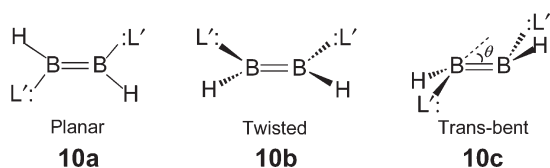
The most intriguing feature of **8** is its planar C(H)B=B(H)C core (Figure 3). The 1.560(18) Å (av) B=B double-bond distance is comparable to those reported for the diborene dianions [from 1.566(9) to 1.636(11) Å],^{31,35,36} to the computed B=B bond distances for OC(H)B=B(H)CO (1.590 Å),³⁷ and to the computed distances in triplet diborene(2) H–B=B–H (1.498–1.515 Å).³⁸ The B=B distance in **8** is 0.27 Å shorter than the B–B single-bond distance in **9** [1.828(4) Å]. While the tetrahedral boron atom in **9** (and **11**) has the formal oxidation state of +2, the trigonal-planar boron atom in **8** (and **10**) bears the formal oxidation state of +1. Interestingly, **10** exhibited polymorphism in the solid state. Computations suggest that carbene-stabilized neutral diborenes favor a planar conformation as observed in **8**. Surprisingly, compound **10** exhibits conformational flexibility through its three polymorphs [i.e., planar **10a**, twisted

10b (18.1° dihedral angle between two CBH planes), and trans-bent **10c** (trans-bending angle $\theta = 36^\circ$); Scheme 6], which may attribute to the flat potential energy surface, the packing effects in crystals, the crystallization conditions, and the size of the NHC ligand.²²

As observed in **8**, **10a**, and **10b**, three-coordinate boron atoms usually adopt a trigonal-planar geometry. Consequently, the pyramidal geometry around the boron atoms in **10c** is noteworthy. These are the first pyramidal three-coordinate boron atoms observed in an acyclic environment.³⁹ The B=B double-bond distances of **10a** [1.602(5) Å] and **10b** [1.582(4) Å], similar to those of **8** and diborene dianions, are about 0.1 Å shorter than that of **10c** [1.679(9) Å]. However, this elongated B=B bond distance in **10c** does not substantially decrease the B–B bond order [Wiberg (1.408) and nonlocalized molecular orbital (NLMO)/natural population analysis (NPA) (1.656) bond indices for the B=B bond in planar **8**; Wiberg (1.445) and NLMO/NPA (1.515) bond indices for the B=B bond in trans-bent **10c**] and thus adds further support for the dictum “the electronic structure, rather than bond distances, determines the nature of multiple bonds”.⁴⁰ The lower-than-2.0 bond orders of these diborenes may be ascribed to the π -back-donation from the boron atoms to the carbenic carbon atoms.⁴¹ Notably, all of the B=B bond distances in **10a**–**10c** are considerably shorter than that [1.795(5) Å] of the corresponding diborene **11**. The B=B double-bond character of **10** is also supported by the $\pi_{B=B} - \pi_{B=B}^*$ absorption ($\lambda_{\max} = 574$ nm). The molecular orbital (MO) study of the simplified models L:(H)B=B(H):L [L: = :C(NHCH)₂] of the planar diborene **8** (Figure 4) and trans-bent diborene **10c** reveals that the B–B π -bonding dominates the highest occupied molecular orbital (HOMO), whereas HOMO–1 has mixed B–B and B–H σ -bonding character.

The ¹¹B NMR spectral study of neutral diborenes **8** and **10**, diboranes **9** and **11**, and borane complexes L:BH₃ and L':BH₃ indicates that with the number of hydrides on the boron atom increases from 1 to 2 and then to 3 and the corresponding ¹¹B resonances are shifted upfield from about +24 ppm (25.30 ppm for **8**; 23.45 ppm for **10**) to about –31.40 ppm (–31.62 ppm for **9**; –31.20 ppm for **11**) and then to about –36.0 ppm (–35.38 ppm for L:BH₃; –36.80 ppm for L':BH₃).^{21,42}

The presence of hydride groups in compounds **8**–**11** has been ascribed to the well-documented alkali-metal-mediated hydrogen abstraction from the solvent.^{43,44} Recently, we discovered that the NHC itself might also serve as the hydride source. The potassium graphite reduction of [L:(NPr₂)Cl]⁺Cl⁻ (**12**; Figure 5a),

Scheme 5. Synthesis of Carbene-Stabilized Neutral Diborene, **8**, and Diborane, **9**Figure 3. Molecular structures of **8** and **9** (hydrogen atoms on carbon are omitted for clarity).Scheme 6. Polymorphic Structures of **10**

prepared by combining ligand **I** with (Prⁱ₂N)BCl₂, did not afford diborene **14**, but compound **13** (Scheme 7) formed instead.²⁰ The strong steric hindrance of the bulky NHC ligand and the diisopropylamino group in **12** may be an important reason for our failure to prepare **14** (Figure 5b).

Borenium **12** contains a three-coordinate, trigonal-planar boron cation (Figure 5a), while the central boron atom in **13** is four-coordinate and adopts a distorted tetrahedral geometry because of the insertion of boron into the benzylic C–H bond of the ligand, forming a six-membered C₄NB cycle (Figure 6). It has been reported that the highly reactive boranediyl intermediate *m*-terphenyl-B: could insert into the C–C bond of the substituent of the *m*-terphenyl ligand.⁴⁵ Notably, the C–B bond distance of 1.599(3) Å in **12** is about 0.05 Å shorter than that in **13** [1.657(2) Å]. The ¹¹B NMR resonance of **12** (30.2 ppm) shifts downfield compared to that of **13** (–12.9 ppm). Both the short C–B bond and the downfield ¹¹B NMR resonance of **12** are in accordance with the electron deficiency of the borenium cation in **12**.

NHC-STABILIZED NEUTRAL Ga₆ OCTAHEDRON

Although the NHC ligands can readily form adducts with gallium halides, the alkali reduction of L:GaCl₃ only led to the isolation of gallium metal powder and a free NHC ligand. Utilizing a different strategy, we reduced the NHC-complexed mesitylgallium dichloride, L':Ga(Mes)Cl₂.⁴⁶ When L':Ga(Mes)Cl₂ was combined with potassium graphite (1:3) in hexane, a pale-yellow [L':Ga(Mes)Cl]₂ dimer, **15**, was isolated. However, the potassium metal reduction of L':Ga(Mes)Cl₂ in toluene (1:2) led to the formation of a ruby-red L':Ga[Ga₄Mes₄]Ga:L'' octahedron, **16**.

The gallium atoms in compound **15**, in the formal gallium oxidation state of +2, are four-coordinate and adopt distorted tetrahedral geometries (Figure 7). The Ga–Ga single bond distance (2.447 Å) in **15** compares well to those (2.425–2.459 Å) in the gallium(II) iodide amine and phosphane complexes.⁴⁷ The formation of compound **16** is quite surprising because its formation involves the unexpected ligand cleavage. The octahedral Ga₆ core in **16** is aggregated by two carbene-coordinated gallium(0) atoms at the axial positions and four Mes-substituted gallium(I) atoms at the equatorial sites (Figure 7). Each of the six gallium atoms is five-coordinate. The fact that the diagonal Ga(3)⋯Ga(3a) distance of 3.443 Å is about 0.2 Å shorter than the Ga(1)⋯Ga(1a) (3.656 Å) and Ga(2)⋯Ga(2a) (3.671 Å) diagonal separations indicates a tetragonal compression⁴⁸ of the Ga₆ octahedron, which is due to the oxidation state difference of the axial gallium(0) atoms and the equatorial gallium(I) atoms.⁴⁹ Three two-fold axes through the Ga(1)⋯Ga(1A),

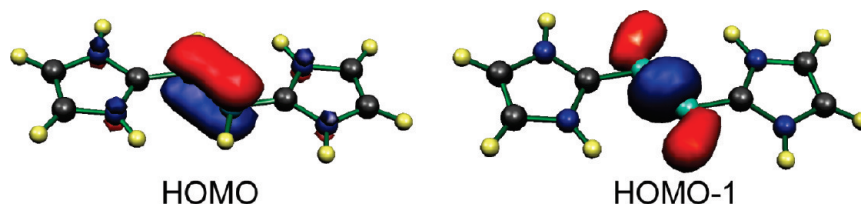


Figure 4. Representations of the frontier orbitals of the simplified model of 8.

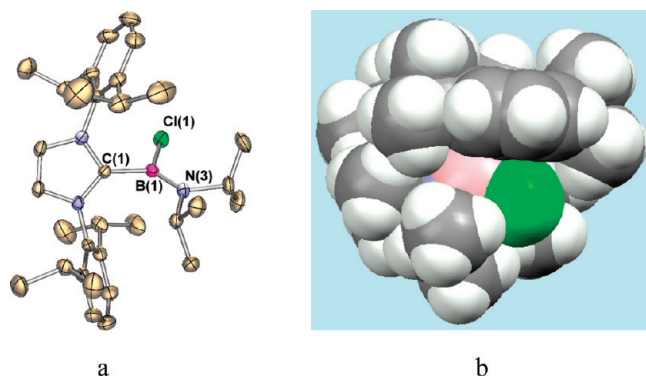
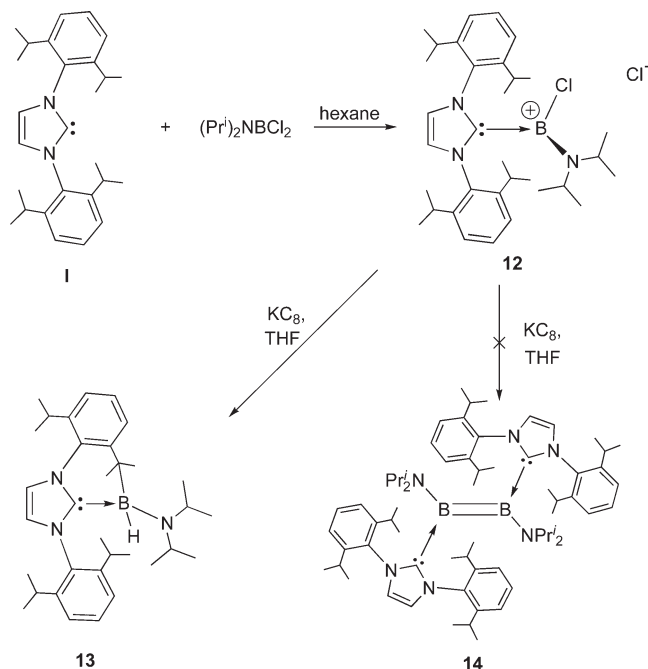


Figure 5. (a) Molecular structure of the **12** cation (thermal ellipsoids represent 30% probability; hydrogen atoms are omitted for clarity). Selected bond distances (Å) and angles (deg): C(1)–B(1) 1.599(3), B(1)–Cl(1) 1.787(3), B(1)–N(3) 1.368(3); C(1)–B(1)–N(3) 126.3(2), C(1)–B(1)–Cl(1) 111.91(18), Cl(1)–B(1)–N(3) 121.79(19). (b) Space filling model of **12**.

Scheme 7. Low-Oxidation-State Boron-Mediated C–H Bond Activation of the NHC Ligand



Ga(2)⋯Ga(2A), and Ga(3)⋯Ga(3A) diagonals constitute the D_2 symmetry of **16**. The nucleus-independent chemical shift (NICS)⁵⁰ value of -10.2 , computed in the cluster center

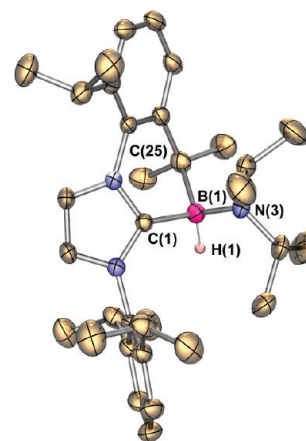


Figure 6. Molecular structure of **13** (thermal ellipsoids represent 30% probability; hydrogen atoms on carbon are omitted for clarity). Selected bond distances (Å) and angles (deg): C(1)–B(1) 1.657(2), C(25)–B(1) 1.689(2), B(1)–H(1) 1.136(15), B(1)–N(3) 1.507(2); C(1)–B(1)–N(3) 116.61(13), C(1)–B(1)–C(25) 100.03(11), C(25)–B(1)–N(3) 116.99(13), C(1)–B(1)–H(1) 106.5(8), C(25)–B(1)–H(1) 106.4(7), N(3)–B(1)–H(1) 109.3(7).

at the PW91PW91/6-311+G** level, confirms the aromatic (metalloaromatic) nature of **16**. The NICS value of -10.2 for **16** is, however, weaker than other group 13 octahedral dianion clusters, such as $[\text{Ga}_6\text{H}_6]^{2-}$ (NICS = -27.3), $[\text{Al}_6\text{H}_6]^{2-}$ (NICS = -25.1), and $[\text{B}_6\text{H}_6]^{2-}$ (NICS = -27.5).⁵¹ Like the isoelectronic $[\text{Ga}_6\{\text{Si}(\text{CMe}_3)_3\}_4(\text{CH}_2\text{C}_6\text{H}_5)_2]^{2-}$ dianion,⁵² **16** bears 14 skeletal electrons and is in accordance with the Wade–Mingos rules.²⁹ Neutral Ga_6R_6 [R = SiMe(SiMe₃)₂]⁵² has only 12 skeletal electrons and thus exhibits a Jahn–Teller-distorted *preclso* octahedral Ga_6 core. In contrast, dianionic $\text{Ga}_6\text{R}_8^{2-}$ [R = Si(C₆H₅)₂Me] shows a planar Ga_6 frame that has been observed in β -gallium.⁵³

The synthesis of **16** prompted us to extend this strategy to other group 13 elements. Thus, we targeted the boron analogue of **16**. However, the potassium reduction of $L''\text{:B}(\text{Ph})\text{Cl}_2$, quantitatively prepared by combining ligand **III** with $\text{B}(\text{Ph})\text{Cl}_2$ in hexane, did not afford the expected boron octahedron but rather a carbene-stabilized $\text{Ph}(\text{H})\text{B}=\text{B}(\text{H})\text{Ph}$ dimer (**17**; Scheme 8).²⁰ X-ray structural analysis of **17** (Figure 8) reveals that the central B–B single bond [1.796(3) Å] is comparable to those in **9** [1.828(4) Å] and **11** [1.795(5) Å]. Since they were first observed in 1990s,⁵⁴ dihydrogen bonds have attracted increasing attention because of their critical roles in molecular aggregation, stabilization of molecular conformations, and proton-transfer reactions.⁵⁵ Interestingly, in **17**, two short intramolecular $[\text{C}–\text{H}^{\delta+} \cdots \text{H}^{\delta-}–\text{B}]$ dihydrogen bonds, namely, 1.871 Å [C(21)–H(21)⋯H(2)–B(2)] and 1.940 Å [C(4)–H(4)⋯H(1)–B(1)], have been

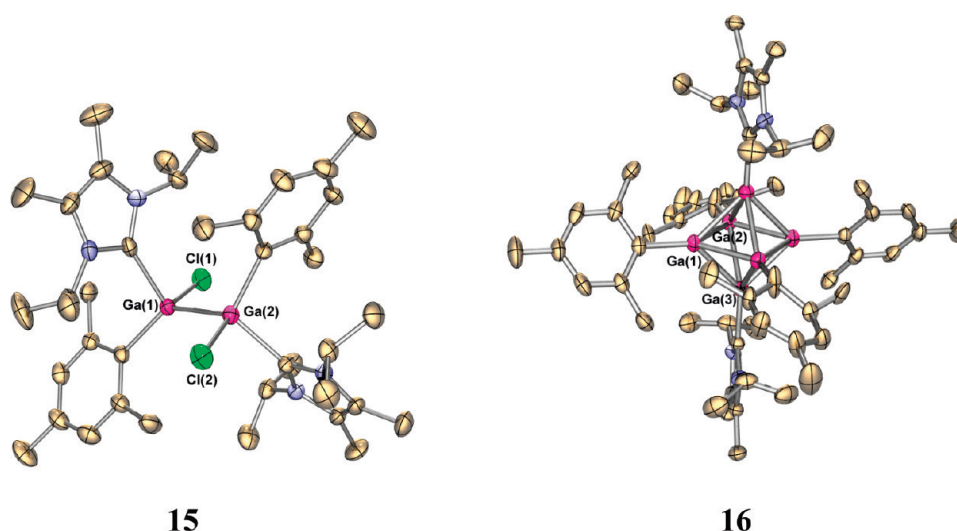


Figure 7. Molecular structures of compounds 15 and 16 (hydrogen atoms are omitted for clarity).

Scheme 8. Synthesis of Compound 17

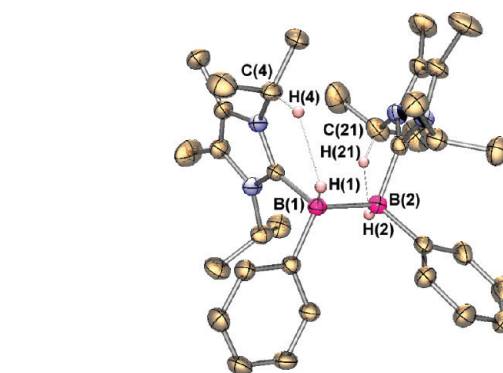
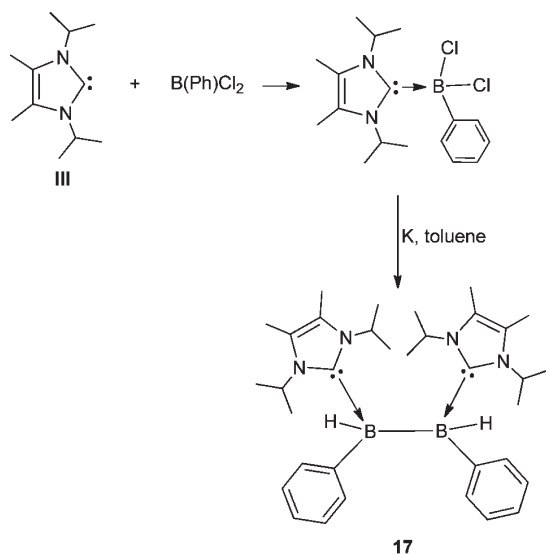


Figure 8. Molecular structure of 17 {thermal ellipsoids represent 30% probability; hydrogen atoms on carbon [except for C(4) and C(21)] are omitted for clarity}. Selected bond distances (Å) and angles (deg): B(1)–B(2) 1.796(3), B(1)–C(1) 1.629(2), B(1)–C(12) 1.637(2), B(1)–H(1) 1.147(16), B(2)–C(18) 1.630(2), B(2)–C(29) 1.631(2), B(2)–H(2) 1.139(16); C(1)–B(1)–B(2) 108.89(12), C(1)–B(1)–C(12) 107.96(12), C(12)–B(1)–B(2) 117.62(12), C(18)–B(2)–B(1) 109.67(12), C(18)–B(2)–C(29) 110.21(13), C(29)–B(2)–B(1) 117.70(13).

observed. Both of them are not only significantly shorter than the sum of the van der Waals radius for the $[C-H^{\delta+} \cdots H^{\delta-}-B]$ system (2.65 Å)⁵⁶ but also shorter than the intramolecular $[C-H^{\delta+} \cdots H^{\delta-}-B]$ dihydrogen bonds observed in 8,9'-[*closo*-[3-Co(η^5 -C₅H₅)]-1,2-C₂B₉H₁₀]₂ (1.994 and 2.097 Å).⁵⁷ These very short intramolecular dihydrogen bonds in 17 may contribute to the gauche conformation adopted by this molecule.

Considering the similar chemical properties between aluminum and gallium, the homologous aluminum octahedron is expected to be isolated. Certainly, with tuning of the electronic and steric properties of the NHC ligands, “carbene stabilization” would be a promising strategy to stabilize intriguing main-group clusters.

NHC-STABILIZED DISILICON AND BIS-SILYLENE

In the well-known low-oxidation-state silicon compounds, disilenes and disilynes, the silicon atoms are in the formal oxidation states of +2 and +1, respectively. Silicon, in its elemental

form (i.e., in the oxidation state of zero), is a ubiquitous semiconductor. Thus, the synthesis of compounds containing silicon atoms in the formal oxidation state of zero is interesting because such silicon(0) compounds may provide a unique platform from which a variety of novel low-oxidation-state silicon compounds may be accessed. The progression from disilene, to disilyne, and then to carbene-stabilized disilicon may be envisioned as a function of the ligand (Scheme 9).

Thus, we investigated the potassium graphite reduction of L: SiCl₄ (3).²³ When 3 was combined with KC₈ (3:KC₈ = 1:4) in THF, only carbene-stabilized disilicon, L:Si=Si:L (18), was isolated as dark-red crystals in 23.2% yield. However, when the potassium graphite reduction of 3 (1:6) was performed in hexane, a carbene-stabilized bis-silylene, L:(Cl)Si–Si(Cl):L (19), was isolated as orange-red crystals. Meanwhile, compound 18 could also be isolated as a minor product. Compound 19 may be regarded as an intermediate of the transformation from 3 to 18. Indeed,

combining **3** with KC_8 ($3:\text{KC}_8 = 1:2$) in toluene results in the isolation of another stable intermediate, $\text{L}:\text{SiCl}_2$ ($\text{L} = \text{I}$).²⁸

Compound **18** (in C_i symmetry) contains an intriguing $:\text{Si}=\text{Si}$: core (Figure 9). The $\text{Si}=\text{Si}$ double-bond distance of **18** [2.230(2) Å] compares well to the reported disilene bond distances (from 2.14 to 2.29 Å)⁵⁸ and the computed (2.249 Å, B3LYP)⁵⁹ and experimental (2.246 Å)⁶⁰ bond distance of Si_2 . However, this value is marginally shorter than that in $\text{OC}:\text{Si}=\text{Si}:\text{CO}$ (2.310 Å, B3LYP)⁶¹ and singlet $\text{Si}_2\text{H}_2^{2-}$ (2.288 Å, B3LYP).⁶² The $\text{Si}-\text{Si}$ double-bond character of **18** is also supported by the $\pi_{\text{Si}=\text{Si}} - \pi^*_{\text{Si}=\text{Si}}$ absorption ($\lambda_{\text{max}} = 468$ nm, in THF), which is within the range of the reported UV absorption maxima (390–480 nm) of stable disilenes.⁵⁸ The ^{29}Si chemical shift of **18** was observed at 224.5 ppm, which compares to the resonances (50–155 ppm) of disilenes.⁵⁸ The X-ray structural data are indispensable in assessing the formal oxidation state of silicon atoms in **18**. The silicon atoms in **18** are only two-coordinate and adopt trans-bent geometries with $\text{C}-\text{Si}-\text{Si}$ angles of $93.57(11)^\circ$. The 1.9271(15) Å $\text{Si}-\text{C}$ bond distance,

Scheme 9. Envisioned Progression from Disilene, to Disilyne, and to Carbene-Stabilized Disilicon

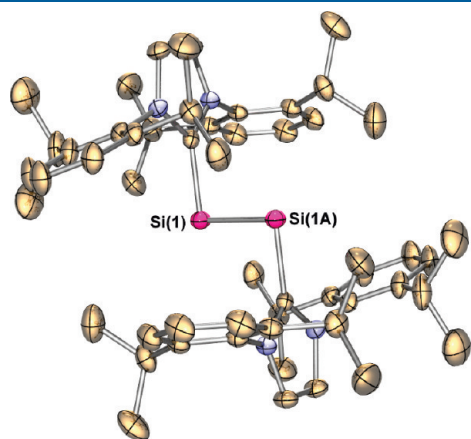
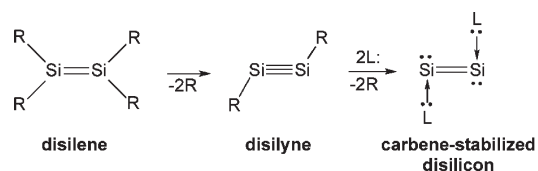


Figure 9. Molecular structure of **18** (hydrogen atoms are omitted for clarity).

similar to that [1.928(2) Å] in $\text{L}:\text{SiCl}_4$, corresponds to a $\text{Si}-\text{C}$ single bond. Moreover, the planes of the imidazole rings of the ligands are perpendicular to the $\text{Si}(1)=\text{Si}(1\text{A})$ vector [the $\text{N}(1)-\text{C}(1)-\text{Si}(1)-\text{Si}(1\text{A})$ torsion angle = 91.01°]. All of these structural features are supportive of $\text{Si}(0)$ atoms in **18**. If the oxidation states of silicon atoms are +2, the $\text{C}_3\text{N}_2\text{Si}_2\text{C}_3\text{N}_2$ core would be expected to be planar with short $\text{C}=\text{Si}$ double bonds and a linear $\text{C}-\text{Si}-\text{Si}-\text{C}$ linkage.⁶³ The almost- 90° trans-bent geometry around the Si_2 core is consistent with a weak hybridization between the 3s and 3p orbitals of silicon atoms in **18**, which is also confirmed by NBO analysis. While the $\text{Si}-\text{Si}$ σ -bond (with 82.2% p character) and π -bond (with 99.6% p character) have mainly p character, the silicon lone-pair orbitals (with 72.8% character) have predominantly s character.²³

Density functional theory (DFT) computations on the simplified $\text{L}:\text{Si}=\text{Si}:\text{L}$ (where L: is $:\text{C}\{\text{N}(\text{C}_6\text{H}_5)\text{CH}_2\}$) model, **18-Ph**, support this bonding analysis.²³ The Wiberg bond index (WBI) of 1.73 supports the presence of a $\text{Si}=\text{Si}$ double bond in **18**. The HOMO corresponds to the $\text{Si}-\text{Si}$ π bond, whereas the HOMO-1 is dominated by the $\text{Si}-\text{Si}$ σ bond. The HOMO-2 is one of the two nonbonding lone-pair MOs (Figure 10). The MO profile of **18-Ph** is quite different from that of the triplet ($X^3\Sigma_g^-$) ground state of the isolated, coordinatively unsaturated, Si_2 molecule, wherein each of the two degenerate $1\pi_u$ MOs are occupied by one electron of the same spin.⁶⁴

Computations suggest that the uncomplexed Si_2Cl_2 molecule adopts a doubly bridged (C_{2v}) $\text{Si}(\mu\text{-Cl})_2\text{Si}$ geometry around 2.361 Å $\text{Si}-\text{Si}$ single bond with a 102.1° dihedral angle between the Si_2Cl rings.²³ In contrast, with the complexation of carbene ligands to the silicon atoms in bis-silylene **19**, the chlorines are not bridging (Figure 11). The two $\text{L}:\text{SiCl}$ fragments are linked via a $\text{Si}-\text{Si}$ single bond (2.393(3) Å) and adopt a gauche conformation (the $\text{Cl}(1)-\text{Si}(1)-\text{Si}(2)-\text{Cl}(2)$ torsion angle is -46.5°). Each three-coordinate $\text{Si}(I)$ atom in **19** adopts a trigonal pyramidal geometry. The bond angle sum of 308.0° (av) at the silicon atoms in **19** compares very well with that in $(t\text{Bu}_2\text{MeSi})_2\text{SiFLi} \cdot (\text{THF})_3$ (307.6°)⁶⁵ and the computed value for $\text{Ph}_2\text{Si}:\text{CNPh}$ (306.8°).⁶⁶ The pyramidal geometry at each silicon atom in **19** results from significant lone electron pair character on both Si atoms. The visible absorption maximum of **19** was observed at $\lambda_{\text{max}} = 510$ nm (in hexane), which is comparable to that ($\lambda_{\text{max}} = 478$ nm) of an intramolecularly base-stabilized three-coordinate silylene.⁶⁷ The ^{29}Si resonance of **19** (38.4 ppm) is between 78.3 ppm of $[\text{C}(\text{H})\text{N}(t\text{Bu})_2]_2\text{Si}$:⁶⁸ and 14.6 ppm of $[\text{PhC}(\text{N}t\text{Bu})_2]_2\text{SiCl}$,⁶⁹ but at a considerably lower field than those (-48.6 to -57.4 ppm) of silylene-isocyanide complexes.⁶⁶

The nature of the bonding in **19** was further probed by B3LYP/6-311+G** DFT computations on the simplified $\text{L}:(\text{Cl})\text{Si}-\text{Si}(\text{Cl})$:

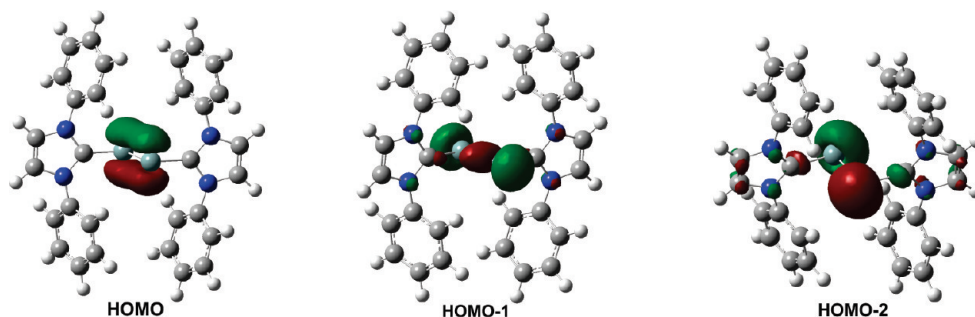


Figure 10. Representation of the HOMO, HOMO-1, and HOMO-2 of **18-Ph**.

L ($L: =:C(NHCH)_2$) model, **19-H**.²³ The localized molecular orbitals (LMOs; Figure 12) reveal a Si–Si σ bonding orbital and two nonbonding lone-pair orbitals, one at each silicon atom. Natural bonding orbital (NBO) analysis indicates that the silicon–silicon σ single bond (WBI = 0.9327) has 12.0% s, 87.5% p, and 0.5% d character, while the nonbonding Si lone pair orbitals have 68.6% s, 31.3% p, and 0.1% d character.

Isolation of the bis-silylene carbene complex **19** also served as a template for subsequent stabilization of bis-silylene by a monoanionic bidentate amidinate ligand (Scheme 10).⁷⁰

Carbene-stabilized digermanium $L:Ge=Ge:L$, isostructural to **18**, has recently been synthesized using the unique $RMg-MgR$ ($R = [(MesNCMe)_2CH]^-$) reducing agent.⁷¹ It should be pointed out that divalent carbon(0) species, $C(NHC)_2$, have also been stabilized by N-heterocyclic carbene ligands,^{72,73} which confirms the theoretical prediction about these types of carbodicarbones.^{74,75} These exciting discoveries suggest a bright future for the application of carbenes in low-oxidation-state main-group chemistry.

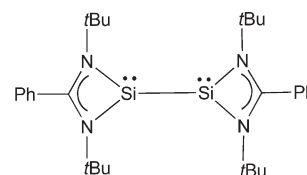
■ NHC-STABILIZED DIPHOSPHORUS (P_2) AND DIARSENIC (As_2)

Phosphorus and arsenic, unlike their lighter congener nitrogen, have extensive allotropy. In contrast to the well-known, metastable tetrahedral allotropes of white phosphorus (P_4) and yellow arsenic (As_4), diatomic allotropes P_2 and As_2 are highly reactive and only persistent at high temperatures.^{76,77} The recent report of mild thermal extrusion of P_2 from niobium diphosphazide complexes indicates that P_2 may be accessed under mild reaction conditions.⁷⁸ The fact that the bond energy of N_2 (226 kcal/mol) is almost twice that of P_2 (116 kcal/mol)⁷⁹ and approaches thrice that of As_2 (83 kcal/mol)⁸⁰ suggests a considerably diminished importance of p– π bonding among third- and fourth-period main-group elements.⁸¹ Thus, E_2 cores

in the corresponding P_2 and As_2 complexes may assume either bonding mode A (triply bonded dipnictogen) or B (singly bonded dipnictinidene) (Scheme 11). Free P_2 and As_2 , assuming bonding mode A, have been reported to function as a four-, six-, or eight-electron-donor ligand ($C-F$; Scheme 11) in transition-metal (M) carbonyl complexes.⁷⁶ The E_2 cores in bonding mode B, featuring four lone electron pairs and unsaturated valence shells, may exhibit both nucleophilic (G)⁸² and electrophilic (H) properties. Inspired by the P_4 - and P_{12} -carbene complexes reported by Bertrand and co-workers,^{83,84} we recently reported the synthesis of carbene-stabilized P_2 ²⁴ and As_2 .²⁵ Both $L:P-P:L$ and $L:As-As:L$ belong to the bonding mode H (Scheme 11).

The potassium graphite reduction of hypervalent phosphorus- or arsenic-carbene complexes **4–6** affords the carbene-stabilized P_2 or As_2 complexes **20–22**, respectively (Scheme 12). Compounds **20–22** were isolated as moisture- and air-sensitive red crystals in moderate yields (**20**, 56.6%; **21**, 20.7%; **22**, 19.2%). The lower yield of the carbene-stabilized As_2 complex **22** indicates the increased synthetic challenge of the heavier dipnictinidene carbene complexes descending group 15. Indeed, carbene-stabilized Sb_2 and Bi_2 have yet to be synthesized.

Scheme 10. Amidinate Ligand-Stabilized Bis-silylene



Scheme 11. Bonding Modes of P_2 and As_2

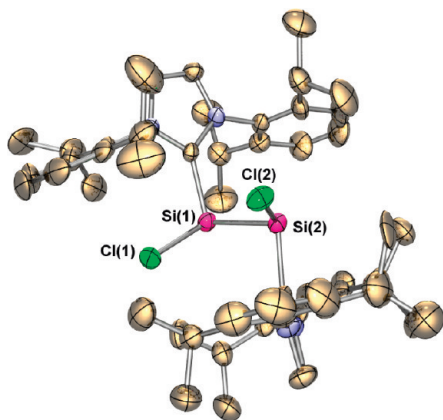
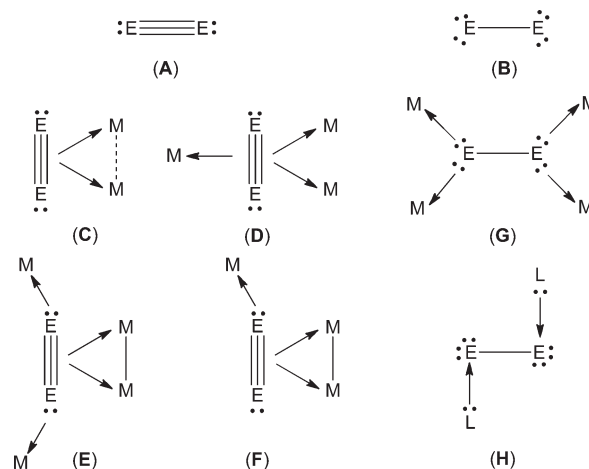


Figure 11. Molecular structure of **19** (hydrogen atoms omitted for clarity).

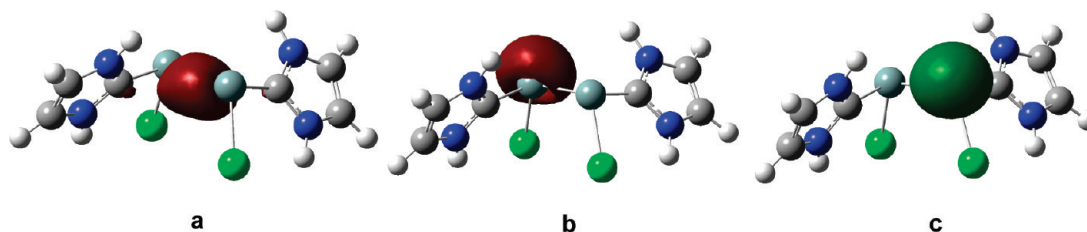
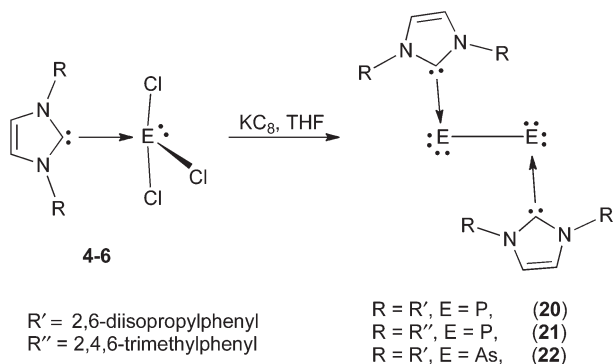


Figure 12. LMOs of the simplified model **19-H**. (a) Si–Si σ -bonding orbital; (b) and (c) lone-pair orbitals.

The X-ray structures of **20** and **21** exhibit similar bond distances but different conformations (Figure 13). While **20**, in C_i symmetry, adopts a trans-bent geometry with a $C(1)-P(1)-P(1A)-C(1A)$ torsion angle of 180.0° , **21** displays a gauche conformation [the $C(1)-P(1)-P(2)-C(22)$ torsion angle is 134.1°]. Moreover, DFT computations at the B3LYP/DZP level on the simplified $L:P-P:L$ [where L : is $:C(NHCH)_2$] model, **20-H**, indicates a C_2 minimum ($C-P-P-C$ torsion angle = 98.6°). This is similar to that of the isolobal equivalent hydrogen persulfide ($H-S-S-H$ torsion angle = 90.6°).⁸⁵ The trend of the $C-P-P-C$ torsion angle change from 180.0° (**20**), to 134.1° (**21**), and then to 98.6° (**20-H**; C_2 minimum) reflects the significant steric effect of the carbene ligands on the conformations of carbene-stabilized P_2 compounds (Scheme 13).

The $P-P$ bond distance of $2.2052(10)$ Å in **20** compares well to typical $P-P$ single bonds. The $C(1)-P(1)-P(1A)$ bond angle [$103.19(6)^\circ$] approaches that of (alkyl)(amino)carbene (CAAC)-stabilized P_2 , **23** [$105.1(2)^\circ$; Scheme 14], which was synthesized by the carbene-induced fragmentation of P_4 .⁸⁶ Interestingly, the two imidazole rings in **20** are almost coplanar to the central P_2 fragment [$N(2)-C(1)-P(1)-P(1A)$ torsion angle = 2.3°], compared to that in **21** (8.2° , av.). The unsymmetrical bisect of the imidazole ring by the $P-C$ bond [with a 18.3° difference between $N(1)-C(1)-P(1)$ and $N(2)-C(1)-P(1)$

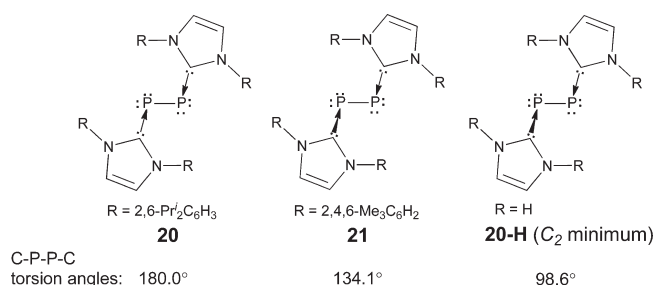
Scheme 12. Synthesis of Carbene-Stabilized P_2 Complexes **20** and **21** and As_2 Complex **22**



angles] may attribute to the steric repulsion between the very bulky carbene ligands. The $P-C$ bond distance [$1.7504(17)$ Å] in **20**, between the $P=C$ double-bond distances ($1.65-1.67$ Å) of the nonconjugated phosphalkenes⁸⁷ and the normal $P-C$ single-bond distance [i.e., the $P-C_{Ph}$ bond distance [$1.839(5)$ Å] in $L:P(Ph)$ ($L: = \text{II}$)],⁸⁸ is about 0.03 Å longer than that [$1.719(7)$ Å] in CAAC-stabilized P_2 (**23**).⁸⁶

Two canonical forms [A (bis-phosphinidene) and B (bis-phosphalkene) in Scheme 15] may be used to interpret the bonding in **20**, **21**, and **23**. Indeed, canonical forms A and B are akin to two resonance forms of carbene phosphinidene adducts.⁸⁹ The low-field ^{31}P chemical shift (54.2 ppm) of **23** is similar to those of the diphosphabutadienes ($34-54$ ppm),⁹⁰ which, coupled with the short $P-C$ bond distance [$1.719(7)$ Å] in **23**, suggests that **23** possesses a 2,3-diphosphabutadiene structure (B). In contrast, the high-field ^{31}P chemical shifts of **20** (-52.4 ppm) and **21** (-73.6 ppm), coupled with the

Scheme 13. Steric Effect of the NHC Ligands on the Conformation of the NHC- P_2 Adduct



Scheme 14. CAAC-Stabilized P_2

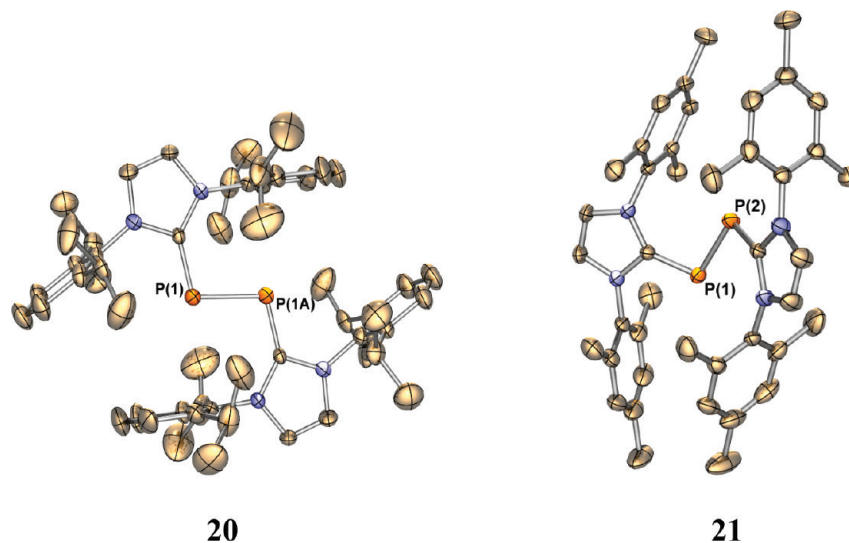
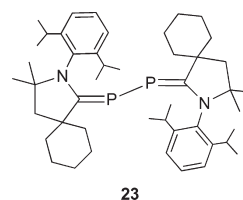


Figure 13. Molecular structure of carbene-stabilized P_2 **20** and **21** (hydrogen atoms are omitted for clarity).

Scheme 15. Canonical Forms of Carbene-Stabilized P₂ Molecules 20, 21, and 23

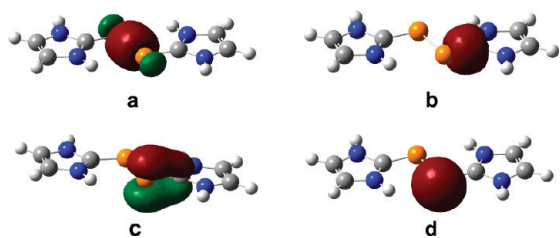
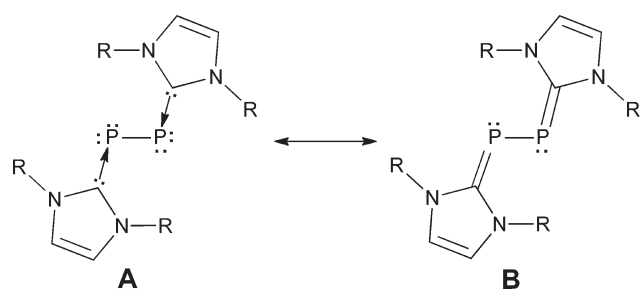


Figure 14. LMOs of the simplified model of **20** (L: = :C(NHCH)₂) with C_i symmetry: (a) P–P σ -bonding orbital; (b) P–C σ -bonding orbital; (c) lone-pair orbital with π back-donation to the empty p orbital of C_{NHC}; (d) lone-pair orbital.

relatively long P–C bond distances (about 1.75 Å), favor **A** as the predominate formulation (Scheme 15). These experimental observations are consistent with the higher electrophilicity of the CAAC ligands than NHCs.⁸⁶

The LMOs of the simplified models [L: = :C(NHCH)₂] of **20** (optimized in C_{2h} symmetry, as shown in Figure 14) and **21** include one P–P σ bond, one P–C σ bond, and two lone-pair orbitals on each phosphorus atom. In terms of NBO analysis, as exemplified in the **20-H** model (C_{2h}), **d** has mainly s character (68.8% s, 31.2% p, and 0.0% d), whereas **c** is essentially pure p (0.0% s, 99.8% p, and 0.2% d). Notably, **c** interacts with the empty p orbital of C_{NHC} via p– π back-donation (involving 64.8% phosphorus and 35.2% carbon components), which, however, is not well developed because of the aromaticity of the imidazole ring (the P–C WBI of 1.397). This bonding description is consistent with the structural features of **20** [i.e., coplanarity of the imidazole ring with the P₂ unit and the 1.7504(17) Å P–C bond distance]. Moreover, the P–P σ single bond (WBI = 1.004) has mainly p character (87.9% p).

Compound **22**, in C_i symmetry, is isostructural to **20** and adopts a trans-bent geometry around the As–As bond [torsion angle of C(1)–As(1)–As(1A)–C(1A) = 180°; Figure 15). This trans-bent conformation may also attribute to the steric repulsion of the ligands because the DFT-optimized structure of the simplified model L:As–As:L (L: = :C(NHCH)₂), **22-H**, favors a gauche conformation with C₂ symmetry (C–As–As–C torsion angle = 93.9°, as shown in Figure 15).²⁵ The central As–As bond distance of 2.442(1) Å is almost the same as that (2.44 Å) in gaseous As₄⁹¹ and compares well to the sum of the arsenic single-bond covalent radii (2.42 Å).⁹² The C(1)–As(1)–As(1A) bond angle of 101.11(5)° is about 2° less than the C(1)–P(1)–P(1A) bond angle in **20** [103.19(6)°], while the As–As bond in **22** is about 0.24 Å longer than the P–P bond in **20** [2.205(1) Å].

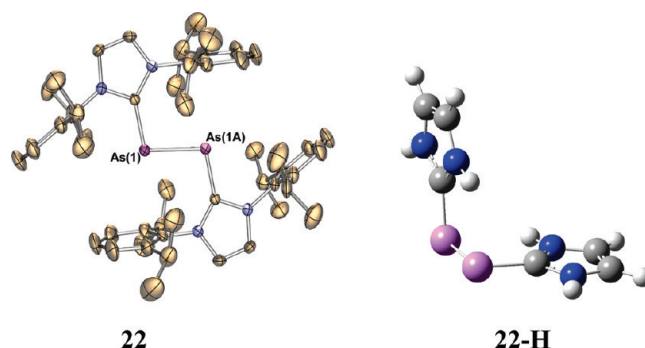
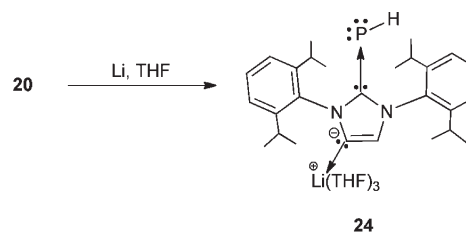


Figure 15. Molecular structure of the carbene-stabilized As₂ complex **22** (hydrogen atoms are omitted for clarity) and the simplified **22-H** model optimized in C₂ symmetry.

Scheme 16. Synthesis of the Carbene-Stabilized Parent Phosphinidene 24



Compound **22** is not only isostructural to the carbene-stabilized P₂ **20**, but also is structurally similar to carbene arseninidene adducts.⁸⁸ Thus, compound **22** may be considered as a diarsinidene complex.

Carbene stabilization denotes a new strategy in approaching the P₂ and As₂ molecules. Furthermore, the reactivity of these molecules should prove interesting. While the electrochemical oxidation of **20**, explored by Bertrand, resulted in a carbene-stabilized P₂²⁺ dication,⁹³ we recently investigated the lithium reduction of **20** (Scheme 16), which results in the isolation of yellow crystals of lithiated-NHC parent phosphinidene adduct, L':P–H (L': = :C{[N(2,6-*i*Pr₂C₆H₃)]₂CHCLi(THF)₃}, **24**.²⁶ Although the mechanism is unclear, the formation of **24** involves both the cleavage of the central P–P bond of **20** and the lithium-mediated C–H activation of the imidazole ring.

The ¹H NMR spectrum of **24** shows that the P–H doublet [δ = 1.86 ppm, ¹J(PH) = 167 Hz] is shifted upfield compared to that of [(CH₃)₂N]₂C=P–H [δ = 3.10 ppm, ¹J(PH) = 159 Hz].⁹⁴ This may be attributed to the stronger net electron-donating ability of the lithiated NHC ligand in **24** than that of the (R₂N)₂C: ligand in [(CH₃)₂N]₂C=P–H. The presence of the P–H fragment in **24** also is unambiguously confirmed by the ¹H-coupled ³¹P NMR spectrum. The ³¹P doublet at –143.0 ppm (¹J = 171 Hz) is upfield when compared to that [δ = –62.6 ppm, ¹J(PH) = 159 Hz] of [(CH₃)₂N]₂C=P–H⁹⁴ and those [δ = 23.8 ppm, ¹J(PH) = 138 Hz; δ = 34.3 ppm, ¹J(PH) = 174 Hz] of P-hydrogeno-C-phosphinophosphaalkenes.⁹⁵

While being between the typical P–C single-bond distances (from 1.83 to 1.88 Å)²⁶ and the reported P=C double-bond distances (1.65–1.67 Å) for the nonconjugated phosphalkenes,⁸⁷ the P–C bond in **24** [1.763(2) Å; Figure 16] compares well to that computed for [CH(CH₃)N]₂CP–H (1.770 Å)⁹⁶ and is slightly longer than the experimental value for [(CH₃)₂N]₂C=P–H [1.740(1) Å].⁹⁷ As a comparison, the P=C double bonds

- (39) Giju, K. T.; Phukan, A. K.; Jemmis, E. D. *Angew. Chem., Int. Ed.* **2003**, *42*, 539–542.
- (40) Xie, Y.; Grev, R. S.; Gu, J.; Schaefer, H. F.; Schleyer, P. v. R.; Su, J.; Li, X.-W.; Robinson, G. H. *J. Am. Chem. Soc.* **1998**, *120*, 3773–3780.
- (41) Scheschkewitz, D. *Angew. Chem., Int. Ed.* **2008**, *47*, 1995–1997.
- (42) Yamaguchi, Y.; Kashiwabara, T.; Ogata, K.; Miura, Y.; Nakamura, Y.; Kobayashi, K.; Ito, T. *Chem. Commun.* **2004**, 2160–2161.
- (43) Garst, J. F. *Acc. Chem. Res.* **1971**, *4*, 400–406.
- (44) Cheng, T. C.; Headley, L.; Halasa, A. F. *J. Am. Chem. Soc.* **1971**, *93*, 1502–1503.
- (45) Grigsby, W. J.; Power, P. P. *J. Am. Chem. Soc.* **1996**, *118*, 7981–7988.
- (46) Quillian, B.; Wei, P.; Wannere, C. S.; Schleyer, P. v. R.; Robinson, G. H. *J. Am. Chem. Soc.* **2009**, *131*, 3168–3169.
- (47) Baker, R. J.; Bettentrup, H.; Jones, C. *Eur. J. Inorg. Chem.* **2003**, 2446–2451.
- (48) Dong, Z.-C.; Corbett, J. D. *Inorg. Chem.* **1996**, *35*, 2301–2306.
- (49) Wolf, R.; Uhl, W. *Angew. Chem., Int. Ed.* **2009**, *48*, 6774–6776.
- (50) Chen, Z.; Wannere, C. S.; Corminboeuf, C.; Puchta, R.; Schleyer, P. v. R. *Chem. Rev.* **2005**, *105*, 3842–3888.
- (51) King, R. B.; Heine, T.; Corminboeuf, C.; Schleyer, P. v. R. *J. Am. Chem. Soc.* **2004**, *126*, 430–431.
- (52) Linti, G.; Coban, S.; Dutta, D. *Z. Anorg. Allg. Chem.* **2004**, *630*, 319–323.
- (53) Donchev, A.; Schnepf, A.; Baum, E.; Stosser, G.; Schnöckel, H. *Z. Anorg. Allg. Chem.* **2002**, *628*, 157–161.
- (54) Wessel, J.; Lee, J. C., Jr.; Peris, E.; Yap, G. P. A.; Fortin, J. B.; Ricci, J. S.; Sini, G.; Albinati, A.; Koetzle, T. F.; Eisenstein, O.; Rheingold, A. L.; Crabtree, R. H. *Angew. Chem., Int. Ed. Engl.* **1995**, *34*, 2507–2509.
- (55) Bakmutov, V. I. *Dihydrogen Bonds: Principles, Experiments, and Applications*; John Wiley & Sons, Inc.: New York, 2008.
- (56) Flores-Parra, A.; Sanchez-Ruiz, S. A.; Guadarrama, C.; Nöth, H.; Contreras, R. *Eur. J. Inorg. Chem.* **1999**, 2069–2073.
- (57) Planas, J. G.; Vinas, C.; Teixidor, F.; Light, M. E.; Hursthouse, M. B. *J. Organomet. Chem.* **2006**, *691*, 3472–3476.
- (58) Weidenbruch, M. In *The Chemistry of Organic Silicon Compounds*; Rappoport, Z., Apeloig, Y., Eds.; Wiley: Chichester, U.K., 2001; Vol. 3; pp 391–428.
- (59) Pak, C.; Rienstra-Kiracofe, J. C.; Schaefer, H. F., III. *J. Phys. Chem. A* **2000**, *104*, 11232–11242.
- (60) Nimlos, M. R.; Harding, L. B.; Ellison, G. B. *J. Chem. Phys.* **1987**, *87*, 5116–24.
- (61) Zhou, M.; Jiang, L.; Xu, Q. *J. Chem. Phys.* **2004**, *121*, 10474–10482.
- (62) Takahashi, M.; Kawazoe, Y. *Organometallics* **2005**, *24*, 2433–2440.
- (63) Dyker, C. A.; Bertrand, G. *Science* **2008**, *321*, 1050–1051.
- (64) Krapp, A.; Bickelhaupt, F. M.; Frenking, G. *Chem.—Eur. J.* **2006**, *12*, 9196–9216.
- (65) Molev, G.; Bravo-Zhivotovskii, D.; Karni, M.; Tumanskii, B.; Botoshansky, M.; Apeloig, Y. *J. Am. Chem. Soc.* **2006**, *128*, 2784–2785.
- (66) Takeda, N.; Suzuki, H.; Tokitoh, N.; Okazaki, R.; Nagase, S. *J. Am. Chem. Soc.* **1997**, *119*, 1456–1457.
- (67) Corriu, R.; Lanneau, G.; Priou, C.; Soulaïrol, F.; Auner, N.; Probst, R.; Conlin, R.; Tan, C. *J. Organomet. Chem.* **1994**, *466*, 55–68.
- (68) Denk, M.; Lennon, R.; Hayashi, R.; West, R.; Belyakov, A. V.; Verne, H. P.; Haaland, A.; Wagner, M.; Metzler, N. *J. Am. Chem. Soc.* **1994**, *116*, 2691–2692.
- (69) So, C.-W.; Roesky, H. W.; Magull, J.; Oswald, R. B. *Angew. Chem., Int. Ed.* **2006**, *45*, 3948–3950.
- (70) Sen, S. S.; Jana, A.; Roesky, H. W.; Schulzke, C. *Angew. Chem., Int. Ed.* **2009**, *48*, 8536–8538.
- (71) Sidiropoulos, A.; Jones, C.; Stasch, A.; Klein, S.; Frenking, G. *Angew. Chem., Int. Ed.* **2009**, *48*, 9701–9704.
- (72) Dyker, C. A.; Lavallo, V.; Donnadiou, B.; Bertrand, G. *Angew. Chem., Int. Ed.* **2008**, *47*, 3206–3209.
- (73) Fuerstner, A.; Alcarazo, M.; Goddard, R.; Lehmann, C. W. *Angew. Chem., Int. Ed.* **2008**, *47*, 3210–3214.
- (74) Tonner, R.; Oexler, F.; Neumueller, B.; Petz, W.; Frenking, G. *Angew. Chem., Int. Ed.* **2006**, *45*, 8038–8042.
- (75) Tonner, R.; Frenking, G. *Angew. Chem., Int. Ed.* **2007**, *46*, 8695–8698.
- (76) Cotton, F. A.; Wilkinson, G.; Bochmann, M.; Murillo, C. *Advanced Inorganic Chemistry*, 6th ed.; Wiley: New York, 1998.
- (77) *Gmelin Handbuch der anorganischen Chemie, Arsen*; Verlag Chemie: Weinheim, Germany, 1952; Vol. 17.
- (78) Piro, N. A.; Figueroa, J. S.; McKellar, J. T.; Cummins, C. C. *Science* **2006**, *313*, 1276–1279.
- (79) Dasent, W. E. *Inorganic Energetics: An Introduction*, 2nd ed; Cambridge University Press: Cambridge, U.K., 1982.
- (80) Mochizuki, Y.; Tanaka, K. *Chem. Phys. Lett.* **1997**, *274*, 264–268.
- (81) Kutzelnigg, W. *Einführung in die Theoretische Chemie*; Wiley-VCH: Weinheim, Germany, 1978; Vol. 2.
- (82) Scherer, O. J.; Ehses, M.; Wolmershauser, G. *Angew. Chem., Int. Ed.* **1998**, *37*, 507–510.
- (83) Masuda, J. D.; Schoeller, W. W.; Donnadiou, B.; Bertrand, G. *Angew. Chem., Int. Ed.* **2007**, *46*, 7052–7055.
- (84) Masuda, J. D.; Schoeller, W. W.; Donnadiou, B.; Bertrand, G. *J. Am. Chem. Soc.* **2007**, *129*, 14180–14181.
- (85) Winnewisser, G.; Winnewisser, M.; Gordy, W. *J. Chem. Phys.* **1968**, *49*, 3465–3478.
- (86) Back, O.; Kuchenbeiser, G.; Donnadiou, B.; Bertrand, G. *Angew. Chem., Int. Ed.* **2009**, *48*, 5530–5533.
- (87) Weber, L. *Eur. J. Inorg. Chem.* **2000**, 2425–2441.
- (88) Arduengo, A. J., III; Calabrese, J. C.; Cowley, A. H.; Dias, H. V. R.; Goerlich, J. R.; Marshall, W. J.; Riegel, B. *Inorg. Chem.* **1997**, *36*, 2151–2158.
- (89) Arduengo, A. J., III; Carmalt, C. J.; Clyburne, J. A. C.; Cowley, A. H.; Pyati, R. *Chem. Commun.* **1997**, 981–982.
- (90) Romanenko, V. D.; Kachkovskaya, L. S.; Markovskii, L. N. *Zh. Obshch. Khim.* **1985**, *55*, 2140–2141.
- (91) Maxwell, L. R.; Hendricks, S. B.; Mosley, V. M. *J. Chem. Phys.* **1935**, *3*, 699–709.
- (92) Pyykkö, P.; Atsumi, M. *Chem.—Eur. J.* **2009**, *15*, 186–197.
- (93) Back, O.; Donnadiou, B.; Parameswaran, P.; Frenking, G.; Bertrand, G. *Nat. Chem.* **2010**, *2*, 369–373.
- (94) Issleib, K.; Leissring, E.; Riemer, M.; Oehme, H. *Z. Chem.* **1983**, *23*, 99–100.
- (95) Bourissou, D.; Canac, Y.; Gornitzka, H.; Marsden, C. J.; Baccaredo, A.; Bertrand, G. *Eur. J. Inorg. Chem.* **1999**, 1479–1488.
- (96) Frison, G.; Sevin, A. *J. Organomet. Chem.* **2002**, *643–644*, 105–111.
- (97) Chernega, A. N.; Antipin, M. Y.; Struchkov, Y. T.; Sarina, T. V.; Romanenko, V. D. *Zh. Strukt. Khim.* **1986**, *27*, 78–82.